Composites Science and Technology 71 (2011) 1110–1116

Contents lists available at ScienceDirect

Composites Science and Technology

journal homepage: www.elsevier.com/locate/compscitech

Determination of strain rate dependent through-thickness tensile properties of textile reinforced thermoplastic composites using L-shaped beam specimens

W. Hufenbach, A. Hornig *, B. Zhou, A. Langkamp, M. Gude

Technische Universität Dresden, Institute of Lightweight Engineering and Polymer Technology (ILK), 01307 Dresden, Holbeinstr. 3, Germany

ARTICLE INFO

Article history:
Received 11 October 2010
Received in revised form 22 March 2011
Accepted 30 March 2011
Available online 5 April 2011

Keywords:
Through-thickness testing
B. Mechanical properties
A. Textile composites
B. Delamination
Strain rate dependency

ABSTRACT

The presented work focuses on a methodology to characterise strain rate dependent strength and elastic properties of textile reinforced composites in laminate through-thickness direction. Here, for the characterisation L-shaped beam specimens are used. The investigated composite is a fabric reinforced thermoplast made of hybrid E-glass/polypropylene yarns. The analytical solution for the determination of the through-thickness tensile strength as proposed by Lekhnitskii and Shivakumar is verified by means of an optical deformation analysis and is extended for thew determination of the through-thickness elastic modulus. Finally, the possibility of the strain rate dependent characterisation is investigated and a Johnson–Cook based modelling approach is used to represent the apparent strain rate dependency of the through-thickness failure onset. The methodology is successfully used to capture the material strain rate effects with the according strength values and model parameters over a strain rate range of $10^{-4}\ s^{-1}$ to $10\ s^{-1}$ as well as the elastic modulus.

1. Introduction

The excellent specific mechanical properties qualify textile reinforced composites for the development and design of material and energy efficient lightweight structures e.g. in vehicle industries and mechanical engineering [1]. With their high energy absorption capacity, thermoplastic matrix based materials are considered to be predestinated for the use in the field of impact resistant design [2]. Recent investigations of this material class mainly deal with the in-plane properties [3–5]. For the reliable structural design however there is a lack of well-founded knowledge of the through-thickness (TT) behaviour of composites, describing the associated TT failure mode delamination especially under highly dynamic loading conditions [6].

The objectives of the presented investigations are therefore to utilise moderately complex and therefore easy to manufacture specimens for the determination of both the tensile strength and elastic properties in TT direction of textile reinforced thermoplastic composites under highly dynamic loading conditions. For the characterisation of the TT properties only sparse investigations exist. A comprehensive overview of possible specimen shapes and the associated testing methods for TT tensile loading is given in [7]. This has also been discussed with the focus on four point curved beam specimen geometry in [8]. Recent work has been published on the quasi-static TT behaviour of epoxy matrix based materials using comparatively small specimens [9,10]. Other investigations deal for instance with the probabilistic investigation of the quasi-static TT performance with waisted short block specimens [11] and the Arcan test device [12].

However, besides waisted coupons and short block specimens, for which the design of the load introduction is always difficult, various testing methods based on Lekhnitskii's solution for the stress distribution in cylindrically orthotropic curved beam sections [13] have been investigated [14] and even standardised [15]. Considering the strain rate dependency of the material less effort has been undertaken to investigate the TT material behaviour. Some experimental work in this field has been done using a Split-Hopkinson-Bar device (see for example [19]) with very small specimens. In [20] the strain rate dependent TT shear behaviour has been studied. Here, due to the coarse textile architecture of the investigated material, the adopted L-beam specimen test setup and procedure with a high-speed camera system was used at elevated testing velocities for the determination of the TT strength $R_r^+(\dot{\varepsilon})$ at different strain rate levels.

With the scope of highly dynamic loading tests, an adequate testing rig was designed and is presented [16], which is based on the determination of interlaminar stresses in L-beam shaped specimens as proposed by Shivakumar [17]. By using optical deformation analysis, this approach can be extended to the determination of the TT elastic modulus in addition to the tensile strength.

* Corresponding author. Tel.: +49 351 463 38007; fax: +49 351 463 38143.
E-mail address: Andreas.Hornig@tu-dresden.de (A. Hornig).
URL: http://www.tu-dresden.de/mw/ilk (A. Hornig).

0266-3538/$ - see front matter © 2011 Elsevier Ltd. All rights reserved.
doi:10.1016/j.compscitech.2011.03.018

Nomenclature

Latin characters

A^R	material constant for strain rate dependency of strength
B	specimen width
d	longitudinal distance of force application
E	Young's modulus
F	force
G	shear modulus
g_M, g_F	dimensionless constants
L	transversal distance of force application
l	specimen arm length
M	momentum
R	strength
R_a, R_i, R_m	specimen outer radius, inner radius, radius of midplane
t	time, specimen thickness
v	loading velocity

Greek characters

β	dimensionless constant
γ	shear strain
ε	normal strain
$\dot{\varepsilon}$	normal strain rate
ζ, η	dimensionless constants
Λ_{r_n}	term to determine E_r at r_n
ν	Poisson's ratio
ω	specimen fixation angle

Superscripts and subscripts

+	tension
1–3	fibre, fibre and through-thickness (TT) direction (bidirectional reinforced textile composites in Cartesian coordinates)
φ, z, r	fibre, fibre and through-thickness (TT) direction (specimen coordinate system, bidirectional reinforced textile composites in cylindrical coordinates)
(*ana*)	analytically determined
fail	failure
max	maximal
n	position over specimen thickness
norm	normalised
(*opt*)	optically determined
(*ref*)	value at reference strain rate

The proposed modus operandi for curved L-beam specimen loaded under uniaxial tension is explained. Firstly, a detailed description of the experimental setup is presented. Based on elastic TT and in-plane parameters, an evaluation of the TT tensile strength $R_3^+ (= R_r^+)$ is performed. For this, the stresses are calculated based on the TT strain field measurements within the experiments. In contrast, the TT stresses can also be determined based on Lekhnitskii solution for cylindrically othotropic materials and the force response under consideration of the experimental and geometric configuration. Additionally, a procedure to determine the TT elastic modulus $E_3 (= E_r)$ is proposed. A Johnson–Cook based [18] modelling approach is used to represent the apparent strain rate dependency of the TT strength.

2. Material specification and specimen manufacture

The investigated composite material is based on a woven fabric: TWINTEX TPP 60 745 supplied by SAINT GOBAIN-VETROTEX. It is a 2/2-twill weave made of hybrid yarns (E-glass/polypropylene). The hot pressing technology was applied to manufacture the L-beam specimen panels in an autoclave. After stacking the unconsolidated fabric between the lower and the upper mould, a moulding fleece and a vacuum bag have been added. Subsequently, the material has been processed with 6 bar at 200 °C. No significant spring back effects were recorded within the demoulding process. The panel was cut into sections of $B = 25$ mm representing the final specimen width (Fig. 1).

The in plane stiffness E_φ was determined before by in-plane tension experiments [4]. The small influence of differing elastic properties in warp and weft direction has been diminished by varying the warp and weft dominated direction in the stacking sequence providing an equally distributed share. The thickness of a single consolidated textile layer equals 0.5 mm resulting in 24 textile layers over specimen thickness $t = 12$ mm ($[0/90]_{24}$). It has been assured, that one of the respective main textile reinforcement directions (warp/weft or 0°/90°) equals the tangential direction in the curved section (index φ, Fig. 2) to assure orthotropy in all directions. TT shear properties have been evaluated using IOSIPESCU testing approach [20]. The material properties and specimen geometry used throughout this study are:

$$E_\varphi = 13{,}700 \text{ MPa} \quad G_{\varphi r} = 1800 \text{ MPa} \quad \nu_{\varphi r} = 0.15$$
$$R_i = 5 \text{ mm} \quad R_a = 17 \text{ mm} \quad R_m = 11 \text{ mm}$$
$$t = 12 \text{ mm} \quad B = 25 \text{ mm} \quad l = 90 \text{ mm}.$$

3. Experimental procedure

3.1. Experimental setup

3.1.1. Test rig

The quasi-static experiments have been performed on a universal testing machine ZWICK Z250 using a 10 kN load cell with a measuring accuracy of ±0.2%. A servohydraulic high velocity test system INSTRON VHS 160/20 has been utilised for the experiments at higher loading velocities to investigate the material behaviour's strain rate dependency. This rig enables tests at high deformation speeds of up to 20 m/s with a load cell accuracy of ±0.5%. The loading fixture (Fig. 2) has been designed to be applicable for both testing machines.

A temporary fixation clamping was integrated to guarantee a non-stressed specimen during the test preparation and an exact specimen angle of 90°. It is removed at the start of the experiments. The specimens are clamped with a torque level of 25 Nm. According to Fig. 2a, the setup parameters are as follows:

$$\omega = 45^\circ \quad d = 28 \text{ mm} \quad L = 72.5 \text{ mm}.$$

3.1.2. Optical deformation measurement

A high-speed camera system and a quasi-static camera in combination with a system for non-contact optical 3D deformation

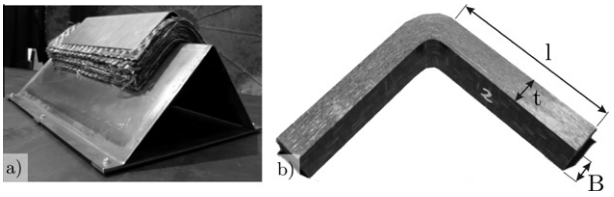

Fig. 1. (a) Specimen manufacturing with 24 plies and a forming tool consisting of upper and lower part (prior to consolidation); (b) final specimen geometry.

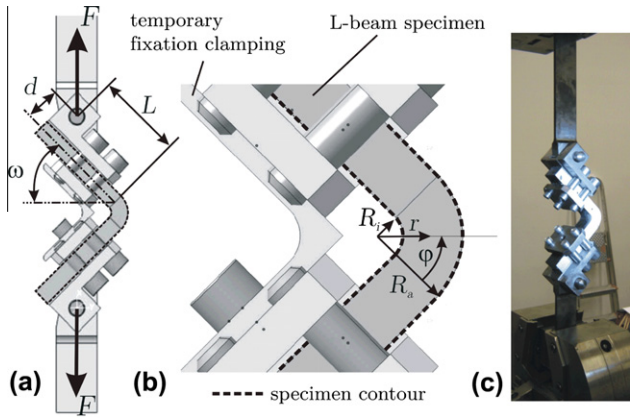

Fig. 2. (a) Loading fixture setup with specimen, (b) detail with parameters used for the analysis, (c) test assembly for experiments with specimen and grey scale pattern (without fixation clamping).

analysis (ARAMIS) was used. With the stochastic grey scale pattern applied on the specimens surface, the gained information on dislocation and distortion fields over specimen thickness are used to calculate the corresponding strain field. Due to the differing camera resolutions (quasi-static: 5 Megapixel; 0.1 and 1 m/s: 54,000 pixel) and the facet size of 15 × 15 pixel with a facet distance of 13 pixel (quasi-static) and 5 pixel (0.1 and 1 m/s), the strain measurement points over specimen thickness differ between 42 (quasi-static) and 10 (0.1 and 1 m/s). Therefore, the strains are averaged in TT direction over 0.29 mm (quasi-static) and 1.2 mm (0.1 and 1 m/s). In Fig 3a–c typical strain fields (ε_r, ε_φ, $\gamma_{r\varphi}$) in the specimen curvature region are shown for a quasi-static test at subcritical loading conditions. The coarse textile architecture of the reinforcement material causes slightly inhomogeneous distributions. Additionally, the principal deformation plot indicates a TT dominated state of strain in the symmetry plane (Fig 3d).

The strain rate

$$\dot{\varepsilon} = \frac{d\varepsilon}{dt}, \tag{1}$$

associated with the stress $\sigma_r(\dot{\varepsilon})$ is determined by the optical measurements at the region of interest and the measurement time step Δt.

3.2. Theoretical background

The relevant mechanical characteristics of the textile reinforced laminate are the in-plane engineering stiffness $E_\varphi = E_1 = E_2$ and in TT direction $E_r = E_3$, as well as the strength in laminate TT direction R_r^+. The calculations are based on plane stress states: $\sigma_z = \tau_{rz} = \tau_{\varphi z} = 0$, where the z-direction represents the specimen width-direction. Also, linear elastic material behaviour is assumed until first failure.

3.2.1. Stress distribution based on strain measurements

The following procedure is proposed to calculate stress components based on the corresponding strain information (ε_r, ε_φ, $\gamma_{r\varphi}$) which are gained via optical measurements in the symmetry plane $\varphi = 90^\circ$ and dependent on the thickness coordinate r.

With given strain information from the experiment, the constitutive equation for rotational orthotropy ($E_r \neq E_\varphi$) under plane state of stress results in

$$\begin{bmatrix} \varepsilon_r \\ \varepsilon_\varphi \\ \gamma_{r\varphi} \end{bmatrix} = \begin{bmatrix} \frac{1}{E_r} & -\frac{\nu_{r\varphi}}{E_r} & 0 \\ -\frac{\nu_{\varphi r}}{E_\varphi} & \frac{1}{E_\varphi} & 0 \\ 0 & 0 & \frac{1}{G_{r\varphi}} \end{bmatrix} \begin{bmatrix} \sigma_r \\ \sigma_\varphi \\ \tau_{r\varphi} \end{bmatrix}, \tag{2}$$

and thus the TT stress components can be calculated, taking the relation of MAXWELL-BETTI $\nu_{r\varphi} = \frac{E_r}{E_\varphi}\nu_{\varphi r}$ into account:

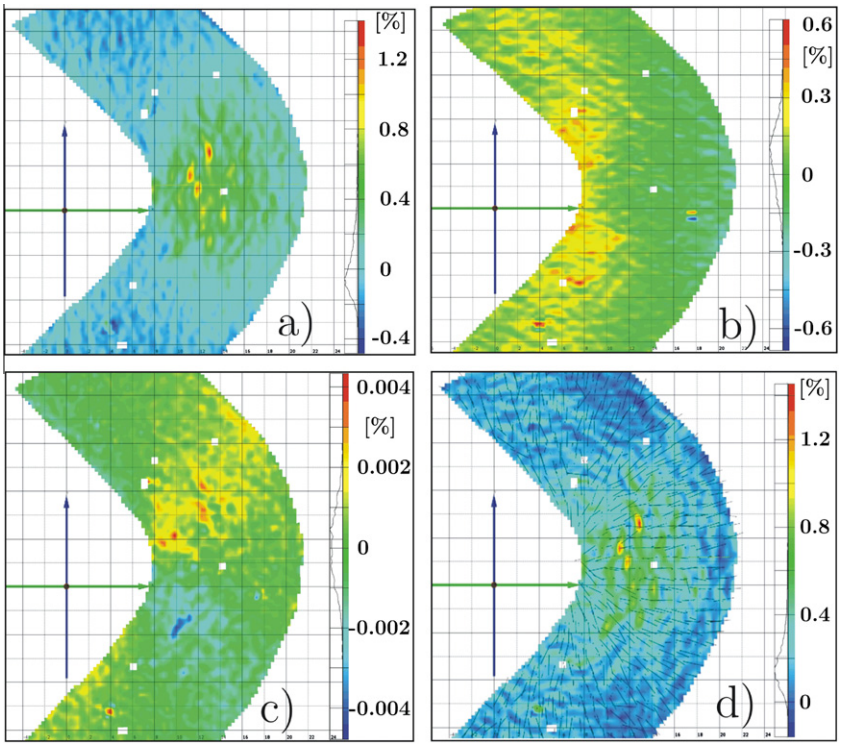

Fig. 3. Via grey scale correlation determined strain field distributions at a non failure relevant load of $F = 100$ N: (a) ε_r, (b) ε_φ, (c) $\gamma_{r\varphi}$ and (d) principal deformations.

$$\sigma_r = \frac{E_r}{1-\nu_{r\varphi}\nu_{\varphi r}}\varepsilon_r + \frac{E_\varphi \nu_{r\varphi}}{1-\nu_{r\varphi}\nu_{\varphi r}}\varepsilon_\varphi,$$
$$\sigma_\varphi = \frac{E_\varphi}{1-\nu_{r\varphi}\nu_{\varphi r}}\varepsilon_\varphi + \frac{E_r \nu_{\varphi r}}{1-\nu_{r\varphi}\nu_{\varphi r}}\varepsilon_r, \quad (3)$$
$$\tau_{r\varphi} = G_{r\varphi}\gamma_{r\varphi}.$$

3.2.2. Stress distribution based on analytical solution

Shivakumar [17] proposed a method for an analytical calculation of the radial, tangential and shear stress distributions $\sigma_r(r)$, $\sigma_\varphi(r)$ and $\tau_{r\varphi}(r)$ respectively in the curved area of the L-beam specimen (Fig. 4) based on Lekhnitskii's equations [13] for the stress distribution in cylindrically othotropic homogeneous curved beams subjected to bending moment M and a tensile load F.

In the specimen curvature symmetry plane $\varphi = \frac{\pi}{2} - \omega$ a uniaxial state of strain is assumed:

$$\varepsilon_\varphi = \gamma_{r\varphi} = 0. \quad (4)$$

Two main aspects have to be considered for the calculation of the stress state with respect to the used test setup. Firstly, an adapted load situation due to the presence of a lever arm loading (length L, Fig. 4) with F has to be comprised. The solution for the L-beam with the tensile load F is split into the solution for a semicircular beam subjected to the load F and the moment M, which can subsequently be treated with Lekhnitskii's solutions. The calculation of the moment accounts for the excentricity of the load initiation at the levers $d \cdot \sin\omega$ and the levers itself $L \cdot \sin\omega$ (Fig. 2):

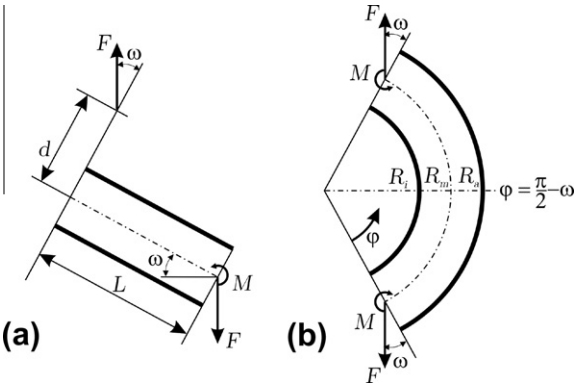

Fig. 4. Mechanical conventions and dimensions of the specimen (a) lever and (b) curved region.

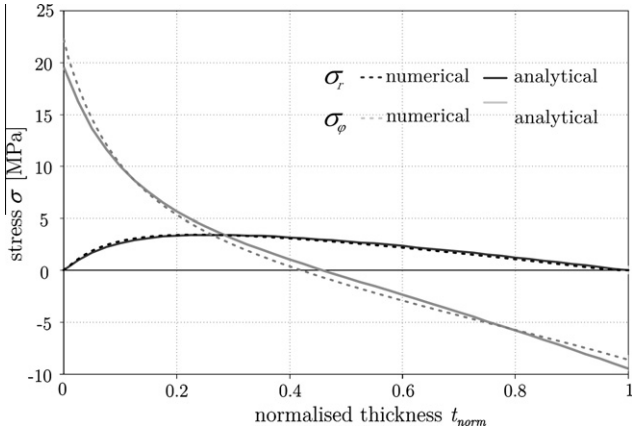

Fig. 5. Comparison of analytically and numerically obtained radial and tangential stress distribution versus the specimen thickness t_{norm} in the specimens symmetry plane $\varphi = \frac{\pi}{2} - \omega$ at $F = 100$.

$$M = F(L\cos\omega - d\sin\omega). \quad (5)$$

Second, a superposition principle is applied, where the contributions of the bending loading (due to the moment M) and tension loading (due to the force F) at the ends of a semicircular beam are taken into account separately:

$$\sigma_r = \sigma_r^M + \sigma_r^F, \quad \sigma_\varphi = \sigma_\varphi^M + \sigma_\varphi^F, \quad \tau_{r\varphi} = \tau_{r\varphi}^M + \tau_{r\varphi}^F. \quad (6)$$

With that, the stress distributions in the curvature at the symmetry plane $\varphi = \frac{\pi}{2} - \omega$ are given by

$$\sigma_r(r) = \frac{M}{R_a^2 B g_M}\left[1 - \frac{1-\zeta^{\eta+1}}{1-\zeta^{2\eta}}\left(\frac{r}{R_a}\right)^{\eta-1} - \frac{1-\zeta^{\eta-1}}{1-\zeta^{2\eta}}\zeta^{\eta+1}\left(\frac{R_a}{r}\right)^{\eta+1}\right] + \frac{F}{rBg_F}\left[\left(\frac{r}{R_a}\right)^{\beta} + \zeta^\beta\left(\frac{R_a}{r}\right)^{\beta} - 1 - \zeta^\beta\right],$$
$$\sigma_\varphi(r) = \frac{M}{R_a^2 B g_M}\left[1 - \frac{1-\zeta^{\eta+1}}{1-\zeta^{2\eta}}\eta\left(\frac{r}{R_a}\right)^{\eta-1} + \frac{1-\zeta^{\eta-1}}{1-\zeta^{2\eta}}\eta\zeta^{\eta+1}\left(\frac{R_a}{r}\right)^{\eta+1}\right], + \frac{F}{rBg_F}\left[(1+\beta)\left(\frac{r}{R_a}\right)^{\beta} + (1-\beta)\zeta^\beta\left(\frac{R_a}{r}\right)^{\beta} - 1 - \zeta^\beta\right],$$
$$\tau_{r\varphi}(r) = 0. \quad (7)$$

with $\zeta = \frac{R_i}{R_a}, \eta = \sqrt{\frac{E_\varphi}{E_r}}, \beta = \sqrt{1 + \frac{E_\varphi}{E_r}(1 - 2\nu_{r\varphi}) + \frac{E_\varphi}{G_{r\varphi}}}$, $g_M = \frac{1-\zeta^2}{2} - \frac{(1-\zeta^{\eta+1})^2}{(\eta+1)(1-\zeta^{2\eta})} - \frac{\zeta^2(1-\zeta^{\eta-1})^2}{(\eta-1)(1-\zeta^{2\eta})}$ and $g_F = \frac{2}{\beta}(1-\zeta^\beta) + (1+\zeta^\beta)\ln\zeta$.

In Fig. 5 the biaxial stress distribution in the symmetry plane section of the L-beam curvature is displayed for $F = 100$ N versus the normalised specimen thickness $t_{norm} = \frac{r-R_i}{t}$, ranging from the inner specimen side (tangentially loaded in tension) $t_{norm} = 0$ to the outer side (loaded in compression) $t_{norm} = 1$. Additionally, these results are compared with numerical investigations for this configuration in Fig. 5. The studies have been performed using ANSYS Classic 11 with 20 orthotropic 2D-disc elements (PLANE182) over the specimen thickness (r-direction) and symmetry boundary conditions at the symmetry plane $\varphi = \frac{\pi}{2} - \omega$. For the maximal radial stress $\sigma_{r\,\max}$, only small deviations of the absolute value ($\leqslant 1\%$) and the position of occurence ($\approx 2.4\%$) can be identified. With the focus on the relevant area $0.1 \leqslant t_{norm} \leqslant 0.9$, the deviation of the tangential stresses σ_φ can be neglected (root deviation 3.5%). The difference at the free edges ($t_{norm} = 0$, $t_{norm} = 1$) does not exceed 12.1%.

3.2.3. Determination of the TT tensile modulus

In contrast to the method proposed in [17], E_r can also experimentally be determined, because strain information are available via the optical inspection. From Eq. (2)

$$E_r\varepsilon_r = \sigma_r - \nu_{r\varphi}\sigma_\varphi \quad (8)$$

.and Eq. (7) a relation for $\varphi = \frac{\pi}{2} - \omega$ is derived, which depends on the experimental values $\varepsilon_\varphi(r)$ at loading stage F (and M, Eq. (5) respectively), the input constants R_i, R_a, E_φ and the required TT tensile modulus E_r only. The simplified expression reads as follows:

$$0 = \Lambda = \frac{M}{g_M}\left[(1-\nu_{r\varphi}) - (1-\eta\nu_{r\varphi})\frac{(1-\zeta^{\eta+1})}{(1-\zeta^{2\eta})}\left(\frac{r}{R_a}\right)^{\eta-1} - (1+\eta\nu_{r\varphi})\frac{\zeta^{\eta+1}(1-\zeta^{\eta-1})}{(1-\zeta^{2\eta})}\left(\frac{R_a}{r}\right)^{\eta+1}\right] - \frac{FR_a}{g_F}\left(\frac{r}{R_a}\right)^{-1}\left[(1-\nu_{r\varphi})(1+\zeta^\beta) - [1-(\beta+1)\nu_{r\varphi}]\left(\frac{r}{R_a}\right)^{\beta} - [1+(\beta-1)\nu_{r\varphi}]\zeta^\beta\left(\frac{R_a}{r}\right)^{\beta}\right] - R_a^2 E_r\varepsilon_r B. \quad (9)$$

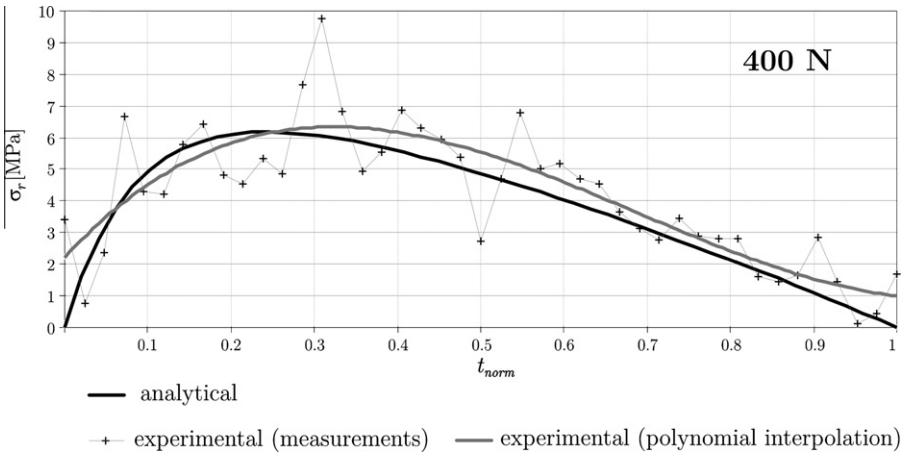

Fig. 6. Comparison of the experimental and analytically determined results at loading state $F = 400$ N.

This equation cannot be solved for E_r explicitly. A solution has to be found numerically based on the strain measurements of ε_r in the experiments for a specific r and loading state F.

4. Results and discussion

The proposed approaches for the calculation of the TT stress distribution σ_r as well as the determination of the TT tensile modulus E_r and strength R_r^+ are experimentally verified and discussed in the following.

4.1. Optical and analytical Lekhnitskii based stress distribution

Eq. (2) is used to calculate the stress distribution $\sigma_r(r)$ based on the experimentally gained strain values $\varepsilon_r(r)$ via grey scale analysis. In contrast to the analytical solution, where uniaxial strain is assumed for an ideal material (Eq. (4)), small amounts of tangential strains ε_φ have been measured in the experiments, contributing to the TT stress state by Eq. (3). A comparison of these two approaches with the average values of three specimens is exemplarily given in Fig. 6 for $F = 400$ N.

The experimental results, approximated with a polynomial function of 4th grade, show a satisfying agreement with the analytical Lekhnitskii solution. The maximum stress is well represented and offers therefore a sufficient basis for TT stress evaluation. The present scatter can be explained by the high material inhomogeneity and reflects the coarse textile architecture with 1870 tex rovings. However, a direct correlation of the alternating stress values with the textile layers or architecture could not be identified. The stress peak at $t_{norm} = 0.3$ is caused by a fibre layup imperfection. The inability of the grey scale correlation technique to identify a representative strain state at free edges causes significant deviations to the analytical solution at the inner and outer radius ($t_{norm} = 0$, $t_{norm} = 1$) of the specimen.

4.2. Quasi-static TT tensile modulus

Three specimen at quasi-static loading conditions have been investigated to determine the TT Modulus E_r, following the proposed modus operandi in Section 3.2. A value can be identified at any position r_n over the specimen thickness if $\Lambda_{r_n} = 0$ (Eq. (9)). For this, 43 strain values $\varepsilon_r(r_n)$ have been analysed ($n = 1,\ldots,43$) at a distinct state of loading F. An example is given in Fig. 7, where the root of $\Lambda_{r_{34}}$ represents E_r at the radius $r_{34} = 14.3$ mm with $F = 500$ N.

The average value of $n = 43$ solutions represents $\bar{E}_r^{n=1,\ldots,43}$ for the given loading state. Finally, this can be analysed for m loading states, where an interval of $\Delta F = 100$ N and $m = 5$ has been chosen here (Table 1).

Table 1
Results for E_r at different loading states F.

F_m (N)	100	200	300	400	500	$\overline{E_r} = 2276$
E_r (MPa)	2274	2313	2249	2290	2254	

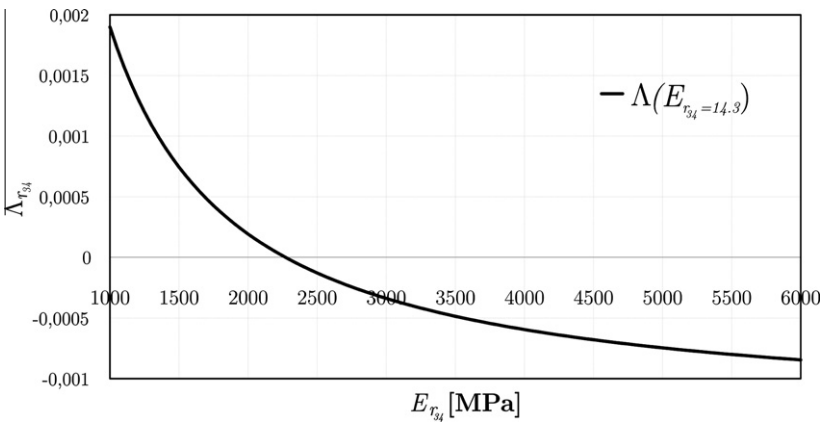

Fig. 7. Determination of E_r by $\Lambda \stackrel{!}{=} 0$ ($\Lambda_{r_{34}}$ with $r_{34} = 14.3$ mm and $F = 500$ N).

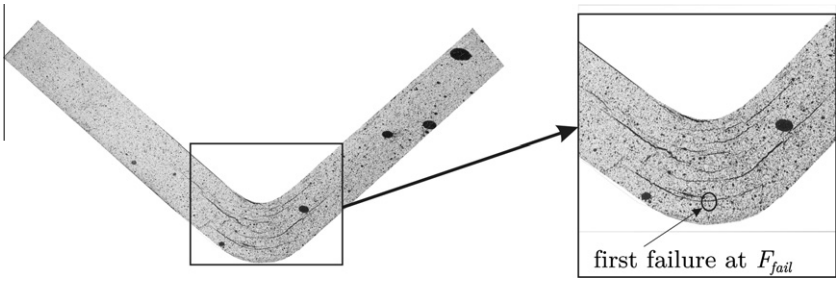

Fig. 8. Failed specimen with indicated first failure location and subsequent delaminations due to continued loading.

Table 2
Results of the experiments at different loading velocities.

Exp.	v (m/s)	F_{fail} (N)	$\dot{\varepsilon}_{fail}$ (s^{-1})	$R_r^{+(opt)}$ (MPa)	$R_r^{+(ana)}$ (MPa)
1		577	0.00015	11.6	8.9
2	3.3×10^{-5}	600	0.00010	12.4	9.3
3		614	0.00006	13.9	9.4
Avg.		597	0.0001	12.6	9.2
4		1484	0.81	48.5	22.7
5	0.1	1135	1.40	36.5	17.4
6		1164	1.01	17.3	17.8
Avg.		1261	1.07	34.1	19.3
8		1489	6.16	36.0	23.0
7	1.0	1914	7.08	39.5	29.3
9		1339	4.02	39.7	20.7
Avg.		1581	5.75	38.4	24.3

Table 3
Model parameters for strain rate dependent TT strength properties.

	A_r^R	$R_r^{+(ref)}$	$\dot{\varepsilon}_r^{(ref)}$ ($\times 10^{-4}$)
Analytical	0.14	9.2	1.10
Optical	0.19	12.6	1.10

The determined mean value of

$$E_r = 2276 \text{ MPa } (S = 1\%) \tag{10}$$

with the standard deviation S correlates well with accompanying studies on tension and compressive specimen in TT direction and is used as input value for the quasi-static calculations in Section 4.1. The assumption of a linear elastic material behaviour in the TT direction is verified by almost constant values for different five loading states.

4.3. Strength properties at elevated loading velocities

Experiments at different loading velocities ($v = 3.3 \times 10^{-5}$, 0.1, 1 m/s) have been executed. The resulting different strain rates over specimen thickness have been determined via the grey scale analysis. A drop in the load history indicates the failure of the material (F_{fail}). Failure always occurs perpendicular to the r-direction as delaminations and are subsequently referred to the tensile strength in TT direction R_r^+ with respect to the curved region Fig. 8. Two ways of the determination are proposed. On the one hand, the strength $R_r^{+(opt)}$ can be experimentally determined by Eq. (3), using the optically measured strain information from the grey scale analysis. $R_r^{+(ana)}$ on the other hand is a purely analytical result based on the force response and Eq. (7) only. Table 2 summaries the conducted experiments and the relevant experimental results. The local strain rate at failure $\dot{\varepsilon}_{fail}$ has been determined in the area of failure just before its occurrence.

The tendency of increasing strengths with a rising strain rate can be clearly identified with both methods. The considerable scatter in the optical measurements is caused by the coarse textile architecture with the resulting non-homogeneous strain distribution and the low high-speed camera resolution. It is likely that matrix or fibre dominated areas with strain concentrations are captured. The slight mismatch in the quasi-static results ($\dot{\varepsilon}_{fail} = 10^{-4}$ s^{-1}) can be explained by the measurement of the present biaxial strain state within the optical analysis. In this case tangential strain contributions are taken also into account, whereas these are neglected in the analytical solution. However, in contrast to the quasi-static investigations, ultimate stress state predictions of the analytical solution differ significantly from the optical results. This effect increases with rising strain rates. An explanation for that can be found in the fact that the analytical solution does

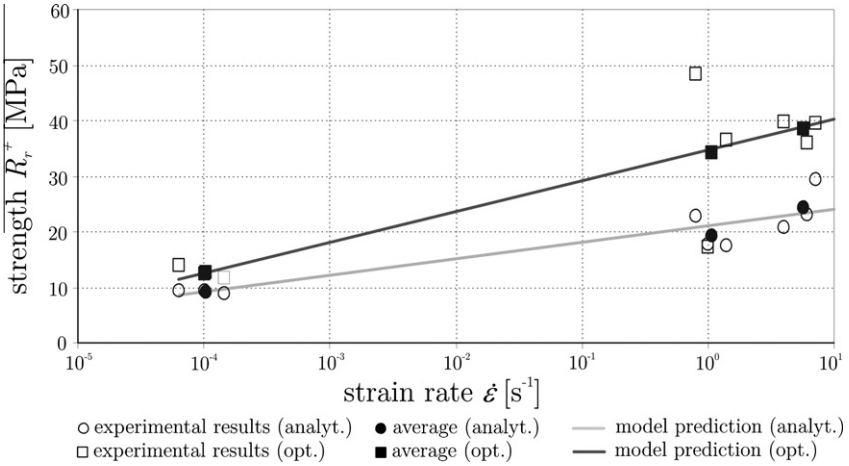

Fig. 9. Comparison of the analytically and optically determined strength values and the model predictions dependent on the strain rate.

not account for the strain rate effects regarding the in-plane properties due to the complexity of the mathematical expression. Additionally, the deviations at higher strain rates might indicate a rising dependency on strain biaxiality at higher strain rates.

The effects of strain rate on the material strength $R_r^+(\dot{\varepsilon})$ within the considered strain rate range was found to be accurately described by the following Johnson–Cook based equation

$$R_r^+(\dot{\varepsilon}_r) = R_r^{+(ref)}\left(1 + A_r^R \ ln\frac{\dot{\varepsilon}_r}{\dot{\varepsilon}_r^{(ref)}}\right), \tag{11}$$

with A_r^R denoting a material constant which controls the linear slope of the model predictions over the strain rate. It can be determined by the best fit approach (Fig. 8). $R_r^{+(ref)}$ is the reference strength at reference strain rate $\dot{\varepsilon}_r^{(ref)}$. The following parameters (Table 3) have been identified to describe the rising strength based on the analytical and the optically measured results.

With the identified parameters for Eq. (11) an adequate estimation for the investigated strain rate range can be achieved (Fig. 9). A comparison of the analytically and optically determined strength values at different strain rates $R_r^{+(ana)}(\dot{\varepsilon})$ and $R_r^{+(opt)}(\dot{\varepsilon})$ with the model predictions is presented in Fig 9. It is worth emphasizing that this type of *natural logarithm*-formulations can result in unreasonable negative values for R_r^+ when values lower than the reference values are requested.

5. Conclusions

A procedure for the determination of through-thickness properties of textile reinforced composite material with L-beam specimens was investigated, which was only used for the identification of the TT strengths in the past. In addition to the well known analytical solution for the stress distribution in such cylindrically othotropic curved beams based on Lekhnitskii, an optical strain field measurement over the specimen thickness has been applied simultaneously. This enables the experimental verification of the analytically predicted stress distribution. A satisfying agreement has been achieved under quasi-static loading conditions. Based on these results, a method for the determination of the elastic TT modulus, has been developed and presented. The measurements on different stress levels indicate a linear elastic TT material response. Additionally, an apparent strain rate dependency of the failure stresses was identified and accurately described by a Johnson–Cook based strain rate model. Further investigation on alternative methods for the determination of strain rate dependent TT properties are planned to evaluate the discrepancy of the proposed analytical and optical evaluation methods. The reduction of the scatter in the results is left open for refinement studies with finer and more homogeneous textile structures.

Acknowledgements

The authors gratefully acknowledge the financial support of this research by the Deutsche Forschungsgemeinschaft (DFG) at the Technische Universität Dresden within the scope of the Collaborative Research Centre (SFB) 639, subproject C4.

References

[1] Hufenbach W, editor, Textile Verbundbauweisen und Fertigungstechnologien für Leichtbaustrukturen des Maschinen- und Fahrzeugbaus. Dresden: Progress Media-Verlag; 2007.
[2] Hufenbach W, Gude M, Ebert C. Hybrid 3D-textile reinforced composites with tailored property profiles for crash and impact applications. Compos Sci Technol 2009;69(9):1422–6.
[3] Brown KA, Brooks R, Warrior NA. The static and high strain rate behaviour of a commingled E-glass/polypropylene woven fabric composite. Compos Sci Technol 2010:272–83.
[4] Böhm R, Gude M, Hufenbach W. A phenomenologically based damage model for textile composites with crimped reinforcement. Compos Sci Technol 2010;70(1):81–7.
[5] Hufenbach W, Böhm R, Thieme M, Winkler A, Mäder E, Rausch J, et al. Polypropylene/glass fibre 3D-textile reinforced composites for automotive applications. Mater Des, in press. doi:10.1016/j.matdes.2010.08.049.
[6] Hufenbach W, Marques FI, Langkamp A, Böhm R, Hornig A. Charpy impact tests on composite structures – an experimental and numerical investigation. Compos Sci Technol 2008;68(12):2391–400.
[7] Lodeiro MJ, Broughton WR, Sims GD. Understanding limitations of through thickness test methods. Plast Rubber Compos 1999;28(9):416–24.
[8] Cui W, Liu T, Len J, Ruo R. Interlaminar tensile strength (ILTS) measurement of woven glass/polyester laminates using four-point curved beam specimen. Compos Part A 1996;27(11):1097–105.
[9] Abot JL, Daniel IM. Through-thickness mechanical characterization of woven fabric composites. J Compos Mater 2004;38(7):543–53.
[10] Daniel IM, Luo J-J, Schubel PM, Werner BT. Interfiber/interlaminar failure of composites under multi-axial states of stress. Compos Sci Technol 2009;69:764–71.
[11] Tagarielli VL, Minisgallo G, McMillan AJ, Petrinic N. The response of a multi-directional composite laminate to through-thickness loading. Compos Sci Technol 2010;70(13):1950–7.
[12] Gning PB, Delsart D, Mortier JM, Coutellier D. Through-thickness strength measurements using Arcan's method. Compos Part B: Eng 2010;41(4):308–16.
[13] Lekhnitskii SG. Anisotropic plates. New York: Gordon & Breach; 1968.
[14] Wisnom Michael R, Jones MI. Delamination due to interaction between curvature induced interlaminar tension and stresses at terminating plies. Compos Struct 1995;32(1–4):615–20.
[15] ASTM international: standard test method for measuring the curved beam strength of a fiber-reinforced polymer–matrix composite ASTM D 6415/D 6415M.
[16] Urban R. Bestimmung der dehnratenabhängigen Eigenschaften in Laminat-Dickenrichtung bei gekrümmter Prüfkörpergeometrie. Term paper (Großer Beleg), TU Dresden, Institute of Lightweight Engineering and Polymer Technology (ILK); 2009.
[17] Shivakumar KN, Allen HG, Avva VS. Interlaminar tension strength of graphite/epoxy composite laminates. AIAA J 1994;32(7).
[18] Johnson GR, Cook WH. Fracture characteristics of three metals subjected to various strains, strain rates, temperatures and pressures. Eng Fract Mech 1985;21(1):S.31–48.
[19] Taniguchi N, Nishiwaki T, Hirayama N, Nishida H, Kawada H. Dynamic tensile properties of carbon fiber composite based on thermoplastic epoxy resin loaded in matrix-dominant directions. Compos Sci Technol 2009;69:207–13.
[20] Hufenbach W, Langkamp A, Hornig A, Ebert C. Experimental determination of the strain rate dependent out-of-plane properties of textile reinforced composites. In: 17th International conference on composite materials (ICCM 17), Edinburgh, United Kingdom; July 27–31, 2009.